Multiscale Registration of Planning CT and Daily Cone Beam CT Images for Adaptive Radiation Therapy

Dana Paquin[*], Doron Levy[†], and Lei Xing[‡]

May 6, 2008

Abstract

Adaptive radiation therapy (ART) is the incorporation of daily images in the radiotherapy treatment process so that the treatment plan can be evaluated and modified to maximize the amount of radiation dose to the tumor while minimizing the amount of radiation delivered to healthy tissue. Registration of planning images with daily images is thus an important component of ART. In this paper, we report our research on multiscale registration of planning CT images with daily CBCT images. The multiscale algorithm is based on the hierarchical multiscale image decomposition of E. Tadmor, S. Nezzar, and L. Vese, *A multiscale image representation using hierarchical* (BV, L^2) *decompositions*, Multiscale Modeling and Simulations, vol. 2, no. 4, pp. 554–579, 2004. Registration is achieved by decomposing the images to be registered into a series of scales using the (BV, L^2) decomposition and initially registering the coarsest scales of the image using a landmark-based registration algorithm. The resulting transformation is then used as a starting point to deformably register the next coarse scales with one another. This procedure is iterated, at each stage using the transformation computed by the previous scale registration as the starting point for the current registration. We present the results of studies of rectum, head-neck, and prostate CT-CBCT registration, and validate our registration method quantitatively using synthetic results in which the exact transformations our known, and qualitatively using clinical deformations in which the exact results are not known.

1   Introduction

Image registration is the process of determining the optimal spatial transformation that brings two images into alignment with one another. More precisely, given two

---

[*]Department of Mathematics, Kenyon College, Gambier, OH 43022-9623 and Department of Mathematics, California Polytechnic State University, San Luis Obispo, CA 93407; paquind@kenyon.edu

[†]Department of Mathematics and Center for Scientific Computation and Mathematical Modeling (CSCAMM), University of Maryland, College Park, MD 20742-4015; dlevy@math.umd.edu

[‡]Department of Radiation Oncology, Stanford University, Stanford, CA 94305-5847; lei@reyes.stanford.edu

images $A(x)$ and $B(x)$, image registration is the process of determining the optimal spatial transformation ϕ such that $A(x)$ and $B(\phi(x))$ are similar. Image registration is necessary, for example, for images taken at different times, from different perspectives, or from different imaging devices. Applications of image registration include image-guided radiation therapy (IGRT), intensity-modulated radiation therapy (IMRT), image-guided surgery, functional MRI analysis, and tumor detection, as well as many non-medical applications, such as computer vision, pattern recognition, and remotely sensed data processing. See [1], [2], [3], [4] for an overview of image registration. Our focus in this paper is registration of computed tomography (CT) and cone beam computed tomography (CBCT) images for image-guided radiation therapy.

Image-guided radiation therapy (IGRT) is the use of patient imaging before and during treatment to increase the accuracy and efficacy of radiation treatment. The goals of IGRT are to increase the radiation dose to the tumor, while minimizing the amount of healthy tissue exposed to radiation. As imaging techniques and external beam radiation delivery methods have advanced, IGRT (used in conjunction with IMRT) has become increasingly important in treating cancer patients. Numerous clinical studies and simulations have demonstrated that such treatments can decrease both the spread of cancer in the patient and reduce healthy tissue complications [5], [6], [7].

IGRT is typically implemented in the following way. CT images are obtained several days or weeks prior to treatment, and are used for planning dose distributions, patient alignment, and radiation beam optimization. Immediately prior to treatment, CBCT images are obtained *in the treatment room* and are used to adjust the treatment parameters to maximize the radiation dose delivered to the tumor. This enables the practitioner to adjust the treatment plan to account for patient movement, tumor growth or movement, and deformation of the surrounding organs. To adjust the patient position and radiation beam angles and intensities based on the information provided by the CBCT images, the CBCT images must first be registered with the planning CT images. Ideally, an adaptive radiotherapy treatment (ART) will eventually be implemented in which the patient alignment and/or radiation beam angles are *continuously updated* in the treatment room to maximize radiation dose to the tumor and minimize radiation to healthy tissue. Such a treatment program would require real-time multi-modality registration of images obtained during treatment with planning images obtained prior to treatment. Thus, accurate registration of images acquired from different machines at different times is an important step in the adaptive treatment process.

In a conventional CT imaging system, a motorized table moves the patient through a circular opening in the imaging device. As the patient passes through the CT system, a source of x-rays rotates around the inside of the circular opening. The x-ray source produces a narrow, fan-shaped beam of x-rays used to irradiate a section of the body. As x-rays pass through the body, they are absorbed or attenuated at different levels, and image slices are reconstructed based on the attenuation process. Three-dimensional images are constructed using a series of two-dimensional slices taken around a single axis of rotation.

In a CBCT imaging system, on the other hand, a cone-shaped beam is rotated around the patient, acquiring images incrementally at various angles around the pa-

tient. The reconstructed data set is a three-dimensional image without slice artifacts, which can then be sliced on any plane for two-dimensional visualization. CBCT images contain low frequency components that are not present in CT images (similar to inhomogeneity related components in magnetic resonance images). One of the challenges in CT-CBCT image registration is thus to account for artifacts and other components that appear in one of the modalities but not in the other. See [8], [9] for a discussion of registration of CT and CBCT images.

In [10], [11], and [12], we presented a series of multiscale registration algorithms that were shown to be particularly effective for registration of *noisy* images. In this paper, we extend our previous work to multiscale registration of CT-CBCT images. The motivation for applying our multiscale registration algorithm to CT-CBCT registration is that artifacts that appear, for example, in CBCT images but not in CT images can be treated in a similar way as noise. Moreover, different anatomical structures in the images to be registered undergo different types of transformations, and thus mapping of the different regions should be approached differently. Our multiscale registration algorithm first registers the coarse scales (such as main shapes, bones, and essential features) of each image, and then uses finer details (such as artifacts and noise) to iteratively refine the resulting transformation.

The structure of this paper is as follows. In Section 2, we briefly discuss ordinary deformable and landmark-based registration algorithms, and present the details of our multiscale registration algorithm. In Section 3, we present several examples to illustrate the accuracy of the multiscale registration technique. Section 4 concludes.

2   Methods

2.1   B-splines deformable registration

Splines-based deformable registration algorithms use a mesh of control points in the images to be registered and a spline function to interpolate transformations away from these points. The basis spline (B-spline) deformation model has the property that the interpolation is locally controlled. Perturbing the position of one control point affects the transformation only in a neighborhood of that point, making the B-splines model particularly useful for describing local deformations. The control points act as parameters of the B-splines deformation model, and the degree of non-rigid deformation which can be modeled depends on the resolution of the mesh of control points. See [13] and [14] for a detailed description of B-splines transformation models. In this paper, we will use a B-splines deformable registration algorithm, in conjunction with the multiscale decomposition and landmark-based registration, with a uniform eight by eight grid of control points chosen automatically.

2.2   Landmark-based registration

Landmark-based registration is an image registration technique which is based on physically matching a finite set of image features. See [4] and [15] for a detailed description of landmark-based registration models. The problem is to determine the transformation such that for a finite set of control points, any control point of the moving image is mapped onto the corresponding control point of the fixed image. More precisely, if A and B are two images to be registered, let $F(A, j)$ and $F(B, j)$, $j = 1, \ldots, m$ be given control points of the images. The solution ϕ of the registration problem is then a map $\phi : \mathbb{R}^2 \to \mathbb{R}^2$ such that

$$F(A, j) = \phi(F(B, j)), \; j = 1, \ldots m.$$

More generally, the solution $\phi : \mathbb{R}^2 \to \mathbb{R}^2$ of the registration problem can be defined to be the transformation ϕ that minimizes the distance

$$D^{LM}(\phi) := \sum_{j=1}^{m} ||F(A, j) - \phi(F(B), j)||^2$$

between the control points.

For the examples presented in this paper, we use an implementation of landmark-based registration in which the transformation ϕ is restricted to translation, rotation, scaling, and shear (i.e. ϕ is an affine transformation). The control points used in the landmark-based registration are chosen manually, and we are currently working on incorporating automatically detected control points in the algorithm.

2.3   Multiscale deformable registration

2.3.1   Hierarchical multiscale image decomposition

The multiscale registration techniques that we developed in [10], [11], [12] are based on the hierarchical (BV, L^2) multiscale image representation of [16]. This multiscale decomposition will provide a hierarchical expansion of an image that separates the essential features of the image (such as large shapes and edges) from the fine scales of the image (such as details and noise). The decomposition is hierarchical in the sense that it will produce a series of expansions of the image that resolve increasingly finer scales, and hence include increasing levels of detail. The mathematical spaces L^2, the space of square-integrable functions, and BV, the space of functions of bounded variation, will be used in the decomposition:

$$L^2 = \left\{ f \;\; | \;\; ||f||_{L^2} := \int f^2 < \infty \right\},$$

$$BV = \left\{ f \;\; | \;\; ||f||_{BV} := \sup_{h \neq 0} |h|^{-1} ||f(\cdot + h) - f(\cdot)||_{L^1} < \infty \right\}.$$

Generally, images can be thought of as being elements of the space $L^2(\mathbb{R}^2)$, while the main features of an image (such as edges) are in the subspace $BV(\mathbb{R}^2)$. The

multiscale image decomposition of [16] interpolates between these spaces, providing a decomposition in which the coarsest scales are elements of BV and the finest scales are elements of L^2. More precisely, the decomposition is given by the following. Define the J-functional $J(f, \lambda)$ as follows:

$$J(f, \lambda) := \inf_{u+v=f} \left(\lambda ||v||_{L^2}^2 + ||u||_{BV} \right), \tag{1}$$

where $\lambda > 0$ is a scaling parameter that separates the L^2 and BV terms. Let $[u_\lambda, v_\lambda]$ denote the minimizer of $J(f, \lambda)$. The BV component, u_λ, captures the coarse features of the image f, while the L^2 component, v_λ (referred to as the residual), captures the finer features of f such as noise. The minimization of $J(f, \lambda)$ is interpreted as a decomposition $f = u_\lambda + v_\lambda$, where u_λ extracts the edges of f and v_λ extracts the textures of f. This interpretation depends on the scale λ, since texture at scale λ consists of edges when viewed under a refined scale. Upon decomposing $f = u_\lambda + v_\lambda$, we proceed to decompose v_λ as follows:

$$v_\lambda = u_{2\lambda} + v_{2\lambda},$$

where

$$[u_{2\lambda}, v_{2\lambda}] = \operatorname*{arginf}_{u+v=v_\lambda} J(v_\lambda, 2\lambda).$$

Thus we obtain a two-scale representation of f given by $f \cong u_\lambda + u_{2\lambda}$. Repeating this process results in the following hierarchical multiscale decomposition of f. Starting with an initial scale $\lambda = \lambda_0$, we obtain an initial decomposition of the image f:

$$f = u_0 + v_0,$$

$$[u_0, v_0] = \operatorname*{arginf}_{u+v=f} J(f, \lambda_0).$$

We then refine this decomposition to obtain

$$v_j = u_{j+1} + v_{j+1},$$

$$[u_{j+1}, v_{j+1}] = \operatorname*{arginf}_{u+v=v_j} J(v_j, \lambda_0 2^{j+1}), \quad j = 0, 1, \ldots$$

After k steps of this process, we have:

$$f = \sum_{j=0}^{k} u_j + v_k, \tag{2}$$

which is a multiscale image decomposition $f \sim u_0 + u_1 + \ldots + u_k$, with a residual v_k. As described in [16], the initial scale λ_0 should capture the smallest oscillatory scale in f, though in practice λ_0 is typically determined experimentally. For the medical images that we have worked with, we have found that $\lambda_0 = 0.01$ works well.
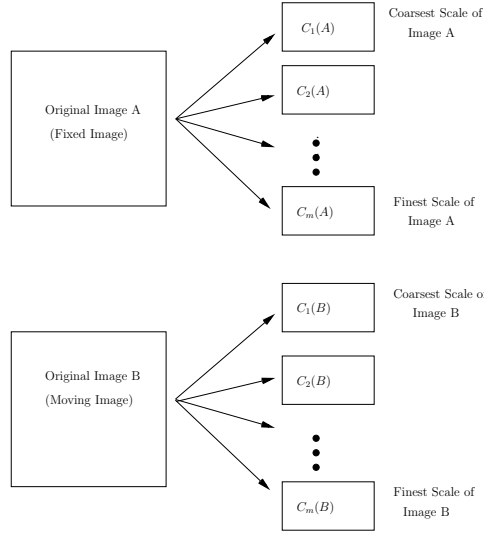
Figure 1: Step 1 of the multiscale registration algorithm: decompose each of the images to be registered into m hierarchical scales.
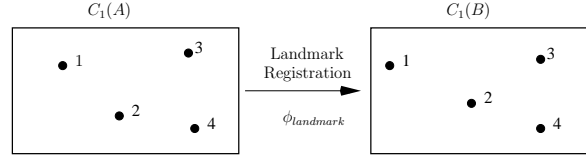

Figure 2: Step 2 of the multiscale registration algorithm: register the coarse scales using a landmark-based registration algorithm.

2.3.2 Multiscale registration algorithm

For the general setup, suppose that we want to register two images A and B with one another. The iterated multiscale registration algorithm is implemented as follows.

1. Apply the multiscale (BV, L^2) decomposition to both images. Let m denote the number of hierarchical scales used in the decomposition. For the registration problems considered here and in our previous work, we use $m = 8$ hierarchical scales in the image decompositions. Let

$$C_k(A) := \sum_{j=0}^{k} u_j$$

   denote the *k-th scale* of the image A. See Figure 1.

2. Register the coarse scales $C_1(A)$ and $C_1(B)$ with one another using a landmark-based registration algorithm. This step allows the practitioner to incorporate known anatomical information about the images to be registered (such as correspondence of bony structures) into the registration process. Let ϕ_{landmark} denote the resulting transformation. See Figure 2.
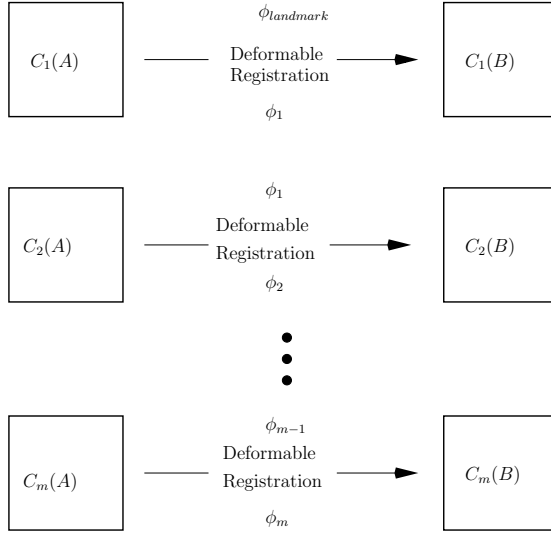
6

Figure 3: Step 3 of the multiscale registration algorithm: iteratively register the scales with one another, at each stage using the previous scale transformation as the starting point for the new registration procedure.

3. Use ϕ_{landmark} as the starting point to deformably register $C_1(A)$ and $C_1(B)$ with one another. This step allows the practitioner to refine the coarse-scale landmark-based transformation obtained in the previous step, while at the same time guaranteeing that the large-scale features (such as bony structures) are still matched with one another. Let ϕ_1 denote the resulting transformation. Next, use ϕ_1 as a starting point to deformably register the next scales $C_2(A)$ and $C_2(B)$ with one another. Let ϕ_2 denote the transformation obtained upon registering $C_2(A)$ with $C_2(B)$. Iterate this method, at each stage using the transformation computed by the previous scale registration algorithm as the starting point for the current registration. Note that the landmark-based registration is only used for registering the coarsest scales of the images; the iterative deformable registration component of the algorithm fine-tunes the registration result obtained with the coarse-scale landmark-based registration. See Figure 3.

See Section 3.3 for a discussion of the computational costs of the multiscale algorithm.

3 Results and Discussion

In this section, we demonstrate the accuracy of the multiscale registration algorithm with image registration experiments using both synthetic and clinical deformations. All of the images used in this section were acquired at the Stanford University Medical Center.

Figure 4: The original and noisy deformed CT images of the rectum.

3.1 Synthetic Results

To quantitatively evaluate the multiscale registration algorithm, we consider several registration problems in which the transformation between the fixed and moving images is known. We consider both rigid and non-rigid deformations.

3.1.1 Rigid Deformations

We begin with a CT image of the rectum, and deform the image using a known transformation. To simulate a rigid transformation, we translate the original CT image 13 mm in the horizontal (X) direction, 17 mm in the vertical (Y) direction, and rotate the image 10 degrees about its center. Finally, to simulate the noise components that appear in CBCT images, we add synthetic multiplicative (speckle) noise to the deformed image. The original CT image and the noisy, deformed image are illustrated in Figure 4.

We repeat this procedure for 50 different CT images of the rectum, and use the multiscale registration algorithm to register the noisy deformed images with the original CT images. The results (X-translation, Y-translation, and rotation angle) of the multiscale registration algorithm are presented graphically in Figure 5; recall that the known deformation parameters are 13 mm in X, 17 mm in Y, and 10 degrees rotation. The results presented in Figure 5 demonstrate that the multiscale registration algorithm accurately recovers the actual deformation parameters.

3.1.2 Non-rigid Deformations

Next, we present a quantitative evaluation of the multiscale algorithm for non-rigid deformations. We begin with a CT image of the rectum, and deform the image using a known non-rigid transformation. To simulate a non-rigid transformation, we deform (warp) the CT image using a known splines vector field deformation by assigning random transformation parameters at each B-spline node of the image. Finally, to simulate the noise components that appear in CBCT images, we add synthetic multiplicative (speckle) noise to the deformed image. We add the same level of noise
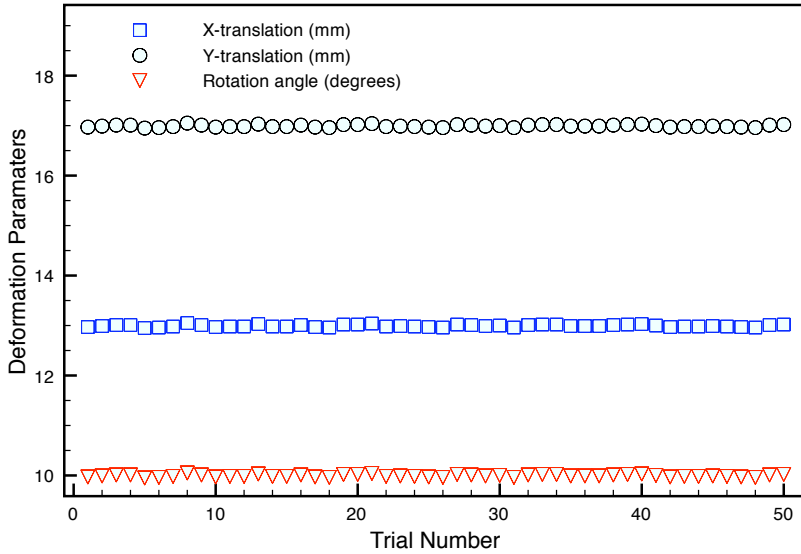
Figure 5: The X-translation, Y-translation, and rotation angle deformation parameters obtained upon registering the noisy deformed rectum images with the CT images using the multiscale registration algorithm.

as that illustrated in Figure 4. In Figure 6, we illustrate the vector deformation field that graphically represents the known deformation between the images. The deformation field represents graphically the magnitude of the deformation at each pixel in the image. Each vector in the deformation field represents the geometric distance between a pixel in the original CT image and the corresponding pixel in the deformed image. Blue corresponds to 0 mm deformation, and red corresponds to 1 mm deformation.

We repeat this procedure for 50 different CT images of the rectum, and use the multiscale registration algorithm to register the noisy deformed images with the original CT images. To quantitatively evaluate the results, we compute the pixel-wise sum of mean square differences (MSDs) between the vector deformation field computed by the multiscale algorithm and the known exact vector deformation field for each pair of images:

$$MSD(C, K) = \frac{1}{N} \sum_{i=1}^{N} (C_i - K_i)^2,$$

where N is the total number of pixels, C_i is the magnitude of the i-th vector in the deformation field computed by the multiscale registration algorithm, and K_i is the magnitude of the i-th vector in the known exact deformation field. If the computed deformation field C and the known deformation field E are exactly the same (i.e. if the multiscale algorithm recovers the exact deformation between the images), then $MSD(C, K) = 0$. Poor matches result in larger values of $MSD(C, K)$. In Table 1, we present the mean, median, minimum, and maximum MSDs obtained upon registering the 50 CT images with the noisy deformed images using the multiscale algorithm. For reference, we also include in Table 1 the mean, median, minimum,
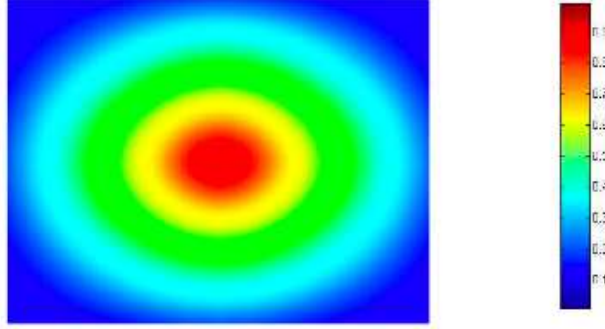
9

Figure 6: The deformation field illustrating the known vector deformation between the original rectum CT image and the noisy deformed image.

	Multiscale MSD: registration of CT images with noisy deformed images	Ordinary MSD: registration of CT images with non-noisy deformed images
Mean	$7.5 \cdot 10^{-4}$	$7.4 \cdot 10^{-4}$
Median	$6.2 \cdot 10^{-4}$	$6.5 \cdot 10^{-4}$
Minimum	$2.3 \cdot 10^{-4}$	$2.3 \cdot 10^{-4}$
Maximum	$8.6 \cdot 10^{-4}$	$8.4 \cdot 10^{-4}$

Table 1: The mean, median, minimum, and maximum MSDs between the computed and known vector deformation fields.

and maximum MSDs obtained upon registering the 50 CT images with the *non-noisy* deformed images using a standard B-splines deformable registration algorithm. Since the B-splines technique has been validated to accurately recover deformations [3], [8], [14], we can use the MSDs obtained with the B-splines algorithm for non-noisy registration as benchmark values for comparison with the multiscale algorithm for noisy registration. We observe that the MSDs obtained upon registering the CT images with the noisy deformed images using the multiscale registration algorithm are similar to those obtained upon registering the CT images with the non-noisy deformed images using a standard B-splines registration algorithm. Thus, we conclude that the multiscale registration algorithm accurately registers the CT images with the noisy deformed images.

3.2 Clinical Results

Next, we present the results obtained with the multiscale registration algorithm for clinical CT-CBCT rectum, head-neck, and prostate registration. In each example, we illustrate a slice of the CT image (upper left), the corresponding slice of the CBCT image (upper right), a checkerboard comparison of the images after ordinary (i.e. non-multiscale) B-splines deformable registration (lower left), and a checkerboard comparison of the images after multiscale registration (lower right). We have high-
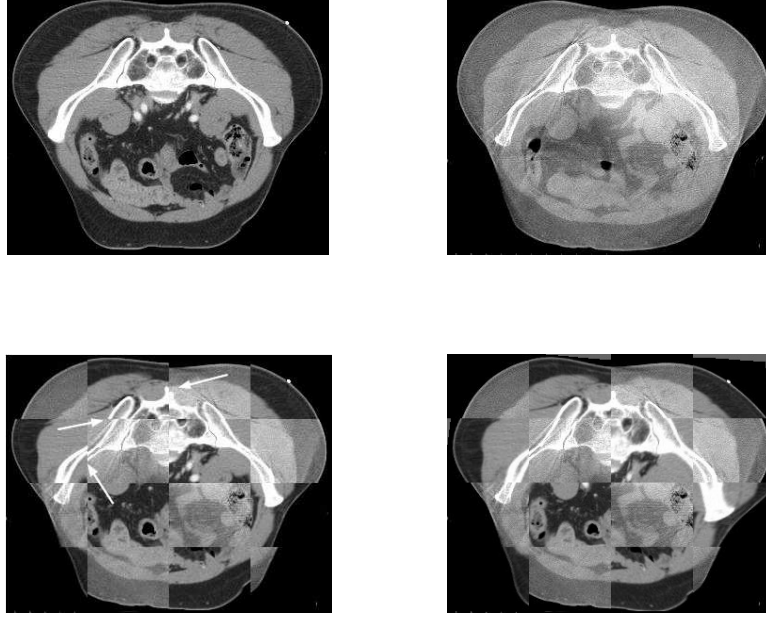
10

Figure 7: Rectum example. Planning CT image (upper left), daily CBCT image (upper right), checkerboard comparison after ordinary B-splines deformable registration (lower left), checkerboard comparison after multiscale registration (lower right). The arrows indicate examples of areas of misalignment between the images after ordinary registration.

lighted areas of misregistration in the checkerboard images after ordinary B-splines registration with arrows. In particular, we notice that misalignment occurs in bony structure regions after ordinary registration, and that we are able to recover this misalignment using the multiscale registration algorithm. The accurate registration of bony structures obtained with multiscale registration is due to the fact that we approach mapping of bony structures differently than mapping of other regions (such as tissue). We first register bony structures with one another using a coarse-scale landmark-based registration, and then use an iterative splines-based registration to refine the result.

To demonstrate the accuracy and applicability of our method, we have illustrated example slices which contain different anatomical features. We performed a total of 50 rectum CT-CBCT registration examples, 50 head-neck CT-CBCT registration examples, and 50 prostate CT-CBCT registration examples. Here, we present the visual registration results for 1 rectum example, 1 head-neck example, and 1 prostate example, and note that the results obtained with all other slices are similar to those presented here.
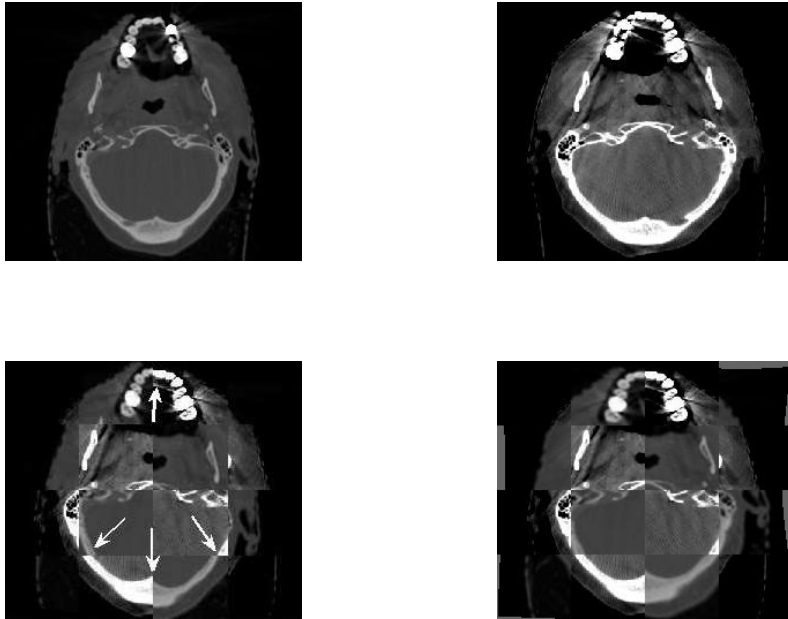
Figure 8: Head and neck example. Planning CT image (upper left), daily CBCT image (upper right), checkerboard comparison after ordinary B-splines deformable registration (lower left), checkerboard comparison after multiscale registration (lower right). The arrows indicate examples of areas of misalignment between the images after ordinary registration.
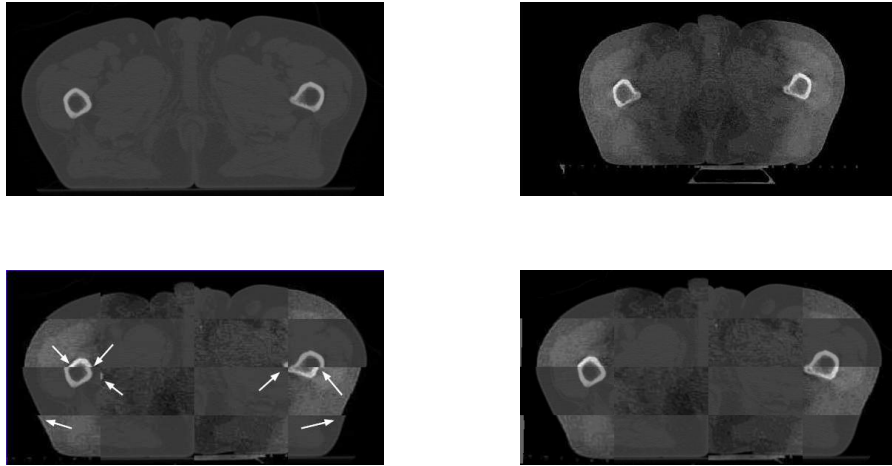
Figure 9: Prostate example. Planning CT image (upper left), daily CBCT image (upper right), checkerboard comparison after ordinary B-splines deformable registration (lower left), checkerboard comparison after multiscale registration (lower right). The arrows indicate examples of areas of misalignment between the images after ordinary registration.

3.2.1 Mutual information similarity measures

In Figure 10, we present the mutual information similarity measures between the planning CT's and daily CBCT's before registration (circles), after ordinary B-splines deformable registration (squares), and after multiscale registration (crosses) for all 50 slices considered for the rectum registration example. The mutual information similarity measures for the head-neck and prostate examples are similar to those presented in Figure 10 for the head-neck example, so we do not include them here. In Table 2, we present the mean mutual information measure (taken over all 50 slices) before registration, after ordinary B-splines registration, and after multiscale registration. For all examples, and for all image slices, the similarity measures increased after multiscale registration, and were slightly higher than the similarity measures after B-splines registration. However, we note that the increased mutual information similarity values do not completely represent the improved accuracy obtained with multiscale registration that we have observed visually in Figures 4-7. Nevertheless, they do capture the qualitative trend of a better matching using our multiscale registration algorithm. See [2], [17] for an overview of the use of mutual information in multi-modality image registration.

3.3 Computation

For all of the examples presented in this paper, computations were performed on a Dell Dimension 8400 Intel Pentium 4 CPU (3.40 GHz, 2.00 GB of RAM). The total time required per slice for the multiscale registration algorithm (including decomposition of the images to be registered) is approximately 30-50 seconds. For the
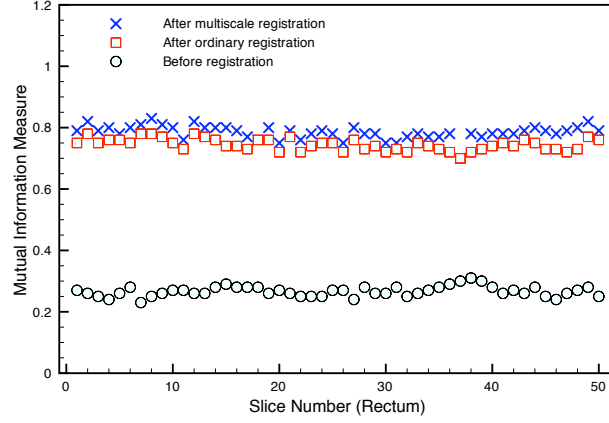
Figure 10: The mutual information similarity measures between the rectum planning CT's and daily CBCT's before registration, after B-splines deformable registration, and after multiscale registration.

Mutual information	Rectum	Prostate	Head-neck
Before registration	0.34	0.21	0.20
After B-splines registration	0.75	0.64	0.74
After multiscale registration	0.79	0.65	0.76

Table 2: The mean mutual information between the planning CT's and daily CBCT's before registration, after B-splines deformable registration, and after multiscale registration.

types of medical images considered here, decomposition of the images (illustrated schematically in Figure 1) into hierarchical scales requires approximately 5 seconds per image. Landmark-based registration of the coarse scales (illustrated schematically in Figure 2) requires approximately 15-20 seconds per image, and iterative deformable registration of all of the remaining scales (illustrated schematically in Figure 3) requires approximately 15-20 seconds. In an ideal implementation of ART, real-time registration of the CT and CBCT images will be performed in the treatment room so that treatment can be continuously updated and optimized; thus, we are currently working on improving the computational efficiency of the multiscale registration algorithm.

The Insight Toolkit (ITK), an open-source software toolkit sponsored by the National Library of Medicine and the National Institutes of Health, was used for the iterative B-splines deformable registration portion of the multiscale registration algorithm. Matlab was used for the multiscale decomposition and for the landmark-based registration.

4   Conclusions

In this paper, we have presented the results of a multiscale registration algorithm for registration of planning CT and daily CBCT medical images. The multiscale algorithm is based on combining the hierarchical multiscale image decomposition of [16] with standard landmark-based and free-form deformable registration techniques. Our hybrid technique allows the practitioner to incorporate *a priori* knowledge of corresponding bony or other anatomical structures into the registration process by using a landmark registration algorithm to register the coarse scales of the fixed and moving images with one another. The transformation produced by this coarse scale landmark registration is then used as the starting point for a multiscale deformable registration in which the remaining scales are iteratively registered with one another, at each stage using the transformation computed by the previous scale registration as the starting point for the current scale registration.

We have demonstrated with several synthetic and clinical image registration experiments that the multiscale registration algorithm is applicable to CT-CBCT registration, which is an important component of ART and IGRT. One of the main features of our multiscale registration algorithm is that it can be used in conjunction with any standard registration technique(s). Thus, the multiscale algorithm can be easily customized to various image registration problems.

References

[1] L. Brown, "A Survey of Image Registration Techniques," ACM Comput. Surv., **24**, 325–376 (1992).

[2] A. Collignon, D. Vadermeulen, P. Suetens, and G. Marchal, "3d multi-modality medical image registration based on information theory," Computat. Imaging Vision, **3**, 263–274 (1995).

[3] W. R. Crum, T. Hartkens, and D. L. G. Hill, "Non-rigid image registration: theory and practice," Br. J. Radiol., **77**, 140–153 (2004).

[4] J. Modersitzki, *Numerical Methods for Image Registration* (Oxford University Press, 2004).

[5] R. Jacob, A. Hanlon, E. Horowitz, et al., "The relationship of increasing radiotherapy dose to reduced distant metastases and mortality in men with prostate cancer," Cancer, **100**, 538–543 (2004).

[6] C.W. Hurkmans, B.C.J. Cho, E. Damen, et al., "Reduction of cardiac and lung complication probabilities after breast irradiation using conformal radiotherapy with or without intensity modulation," Radiother. Oncol., **62**, 163–171 (2002).

[7] M. Tubiana and F. Eschwege, "Conformal radiotherapy and intensity-modulated radiotherapy: Clinical data," Acta Oncol., **39**, 555-567 (2000).

[8] J. Lawson, E. Schreibmann, A. Jani, and T. Fox, "Quantitative evaluation of a cone-beam computed tomography-planning computed tomography deformable image registration method for adaptive radiation therapy," J. Appl. Clin. Med. Phys., **8**, 96–113 (2007).

[9] J. Nord, H. Helminen, "Inter-fraction deformable registration of CT and Cone Beam CT images for adaptive radiotherapy," Proc. 2005 Finnish Sig. Proc. Symp. (2005).

[10] D. Paquin, D. Levy, E. Schreibmann, and L. Xing, "Multiscale image registration," Math. Biosci. Eng., **3**, 389–418 (2006).

[11] D. Paquin, D. Levy, and L. Xing, "Multiscale deformable registration of noisy medical images," Math. Biosci. Eng., **5**, 125–144 (2008).

[12] D. Paquin, D. Levy, and L. Xing, "Hybrid multiscale landmark and deformable image registration," Math. Biosci. Eng, **4**, 711–737 (2007).

[13] S. Lee, G. Wolberg, K.-Y. Chwa, and S. Y. Shin, "Image metamorphosis with scattered feature constraints," IEEE T. Vis. Comput. Gr., **2**, 337–354, (1996).

[14] S. Lee, G. Wolberg, and S. Y. Shin, "Scattered data interpolation with multilevel B-splines," IEEE T. Vis. Comput. Gr., **3**, 228–244 (1997).

[15] K. Rohr, *Landmark-based Image Analysis*, (Kluwer Academic Publishers, Dordrecht, 2001).

[16] E. Tadmor, S. Nezzar, and L. Vese, "A multiscale image representation using hierarchical (BV, L^2) decompositions," Multiscale Model. Sim., **2**, 554–579 (2004).

[17] P. Viola, W. Wells, H. Atsumi, S. Nakajima, and R. Kikinis, "Multi-modal volume registration by maximization of mutual information," Med. Image Anal., **1**, 35–51 (1995).